Segregation of Mg at TiB$_2$/Al interface mitigating the Zr-poisoning effect

Shihao Wang [a,b,c,*], Yun Wang [c], Yijie Zhang [c], Feng Wang [c], Teruo Hashimoto [d], Xiaorong Zhou [d], Zhongyun Fan [c], Quentin Ramasse [a,b]

[a] *SuperSTEM Laboratory, SciTech Daresbury Campus, Daresbury WA4 4AD, UK*
[b] *School of Chemical and Process Engineering, University of Leeds, Leeds LS2 9JT, UK*
[c] *BCAST, Brunel University London, Uxbridge, Middlesex UB8 3PH, UK*
[d] *School of Materials, University of Manchester, Manchester M13 9PL, UK*

A B S T R A C T

Interfacial segregation can modify a substrate's heterogeneous-nucleation potency. In Al alloys inoculated with TiB$_2$, for instance, Zr segregation degrades TiB$_2$'s nucleation potency and causes the loss of grain refinement, a phenomenon termed the Zr-poisoning effect. Here we use grain-refining tests to demonstrate that the addition of Mg can revive grain refinement from the Zr-poisoning effect. Using advanced transmission electron microscopy, we identify the segregation of Mg at the TiB$_2$/Al interface, which causes the disappearance of the poisoning Ti$_2$Zr two-dimensional compound (2DC). In its place, atomic layers of a nature close to the Al solid, which we term "Al-like layers", develop, rendering the TiB$_2$ potent again to catalyse the nucleation of α-Al. Thereby, Mg-segregation-modified TiB$_2$ particles are reactivated for heterogeneous nucleation of Al grains. Apart from a mitigation of the Zr-poisoning effect, this work may shed further light on the manipulation of heterogeneous nucleation by atomic engineering of the nucleating substrate.

Main

Grain refinement is essential in aluminium (Al) alloys for improvements in aspects of casting integrity, alloy microstructure, mechanical properties, and processability for downstream thermomechanical processing [1–3]. To obtain grain refinement, chemical inoculation is the most practical and widely used method in Al foundries, for which Al-5Ti-1B master alloy is one of the most successful grain refiners developed over many decades [4,5]. Despite its practical success, the mechanism underpinning its effectiveness has been disputed for a long time; several theories were proposed, with no clear consensus emerging [6–14]. The advent of advanced (scanning) transmission electron microscopy (S/TEM) in combination with powerful computational methods has offered unprecedented insights into the mechanism and its roots at the TiB$_2$/Al interface: it identified the so-called Al$_3$Ti 2DC as a key interfacial segregation layer that modifies TiB$_2$ and enhances its potency to nucleate α-Al grains [14–18]. Such interface can be further manipulated by the segregation of Zr or Si, which was revealed as the cause of observed Zr- and Si-poisoning effects [19–21]. Realising the importance of TiB$_2$/Al interfaces, Li *et al.* intentionally doped TiB$_2$ particles with solute C, the segregation of which turned out to greatly

remove the Si- and Zr- poisoning effects [22]. Thus, a general concept of atomic engineering of the substrate/metal interface emerges as a strategy to manipulate heterogeneous nucleation by modifying the structural and chemical compatibility at the interface. This has now also been realised in substrate/metal systems other than TiB$_2$/Al, such as MgO/Mg [23–25], γAl$_2$O$_3$/Al [24–26], and αAl$_2$O$_3$/Al [27,28], to alter accordingly the heterogeneous nucleation behaviour.

Grain-refining test results in the literature suggest that, like C, Mg could be a solute candidate to alleviate the Zr-poisoning effect through atomic-level engineering of interfacial segregation. It was observed by Birch and Fisher that Mg can counteract the Zr-poisoning effect [29]. And in contrast to the catastrophic loss of grain refinement in commercial purity (CP) Al [19], Al-5Zn-1.5Mg, AA7050 and AA7055 alloys were shown to experience a relatively mild Zr-poisoning effect [30,31]. Similarly, the addition of 0.13 wt.% Zr into both Al-2.5Cu-2.5Mg and Al-6.5Zn-2.5Mg with 0.2 wt.% Al-3Ti-1B inoculation only caused small increases in grain size [32]. Although these Al alloys all contain Mg, we cannot conclude from a sole heterogeneous nucleation perspective that the interfacial segregation of Mg rejuvenates TiB$_2$ substrates' potency. An alternative explanation could be that the solute's contribution to growth restriction acts as the dominant factor mitigating the

---

Zr-poisoning effect. Both mechanisms may also work synergistically. More experimental work is therefore required to verify the role of Mg. This motivated the present work to answer the following questions: *i)* does the addition of Mg revive grain refinement from the Zr-poisoning effect? *ii)* can Mg segregate to the TiB$_2$/Al interface? *iii)* what is the atomic modification at the interface, if any? *iv)* how is heterogeneous nucleation modified? And *v)* what is the mechanism of grain refinement?

Experimental methods are provided in the supplementary material. The raw materials and master alloys are given in Table S1. To study the effect of alloy compositions (in wt.% unless otherwise specified) on the performance of Al-5Ti-1B, a series of grain refining tests were carried out, with samples listed in Table S2. Each test sample was named according to the added materials and their sequences in the casting experiments. Electron microscopy was used post-mortem to investigate any atomic modifications at the TiB$_2$/Al interface for which the changes in grain refining performance were observed. TEM specimens were prepared from the representative samples: Al-0.2Al5Ti1B, Al-0.1Zr-0.2Al5Ti1B, and Al-0.1Zr-0.2Al5Ti1B-1Mg.

Fig. 1 demonstrates as a control experiment the now well-known effects of interfacial segregation on the grain-refining capability of TiB$_2$ inoculation. As expected, the addition of 0.2 % Al-5Ti-1B drastically refines the grain structure of CP Al after solidification (Fig. 1(a)), which is attributed to the exceeding nucleation potency of the added TiB$_2$ particles that have an Al$_3$Ti 2DC segregation layer on their basal

surface ([17], Fig. 1(d)). In contrast, a poisoning effect occurs when 0.1Zr is present in the melt, as coarse and columnar grains appear in the solidified Al-0.1Zr-0.2Al5Ti1B ingot (Fig. 1(b)). As shown by the high-angle annular dark field (HAADF) STEM image in Fig. 1(e), Zr is found concentrated at the interface between the TiB$_2$ basal plane and Al (quoted as TiB$_2$/Al unless specified otherwise), forming the so-called Ti$_2$Zr 2DC monolayer [19] that poisons the potency of TiB$_2$. Strikingly, a further addition of 1 % Mg appears to counteract the Zr-posoning effect, reviving grain refinement in the cast sample of Al-0.1Zr-0.2Al5Ti1B-1Mg (Fig. 1(c)). At the corresponding TiB$_2$/Al interface, neither Al$_3$Ti 2DC nor Ti$_2$Zr 2DC is observed (Fig. 1(f)). Two atomic layers of faint contrast are found instead. Further STEM-EDS mapping in Fig. 1(g) finds that they are spatially correlated to the areas where Mg is concentrated whilst the segregation of Zr at the interface disappears. A possible conclusion is thus that Mg can segregate to the TiB$_2$/Al interface and restore grain refinement in Al-0.1Zr-0.2Al5Ti1B-1Mg from the Zr-poisoning effect.

More grain-refining-test results in Figs. S1 and S2 indicate that either the Zr-poisoning or the mitigation behaviour is not affected by the addition sequence. When grain refinement is regained, TiB$_2$ particles were repeatedly observed within Al grains (around 200 µm on average) in Al-0.1Zr-0.2Al5Ti1B-1Mg, with an example shown in Fig. S3. The TiB$_2$ particles remain as hexagonal plates in morphology and follow a log-normal size distribution (Fig. S4). In comparison with previous reports [17,19,33,34], additions of 0.1 % Zr and 1 % Mg into the Al melt
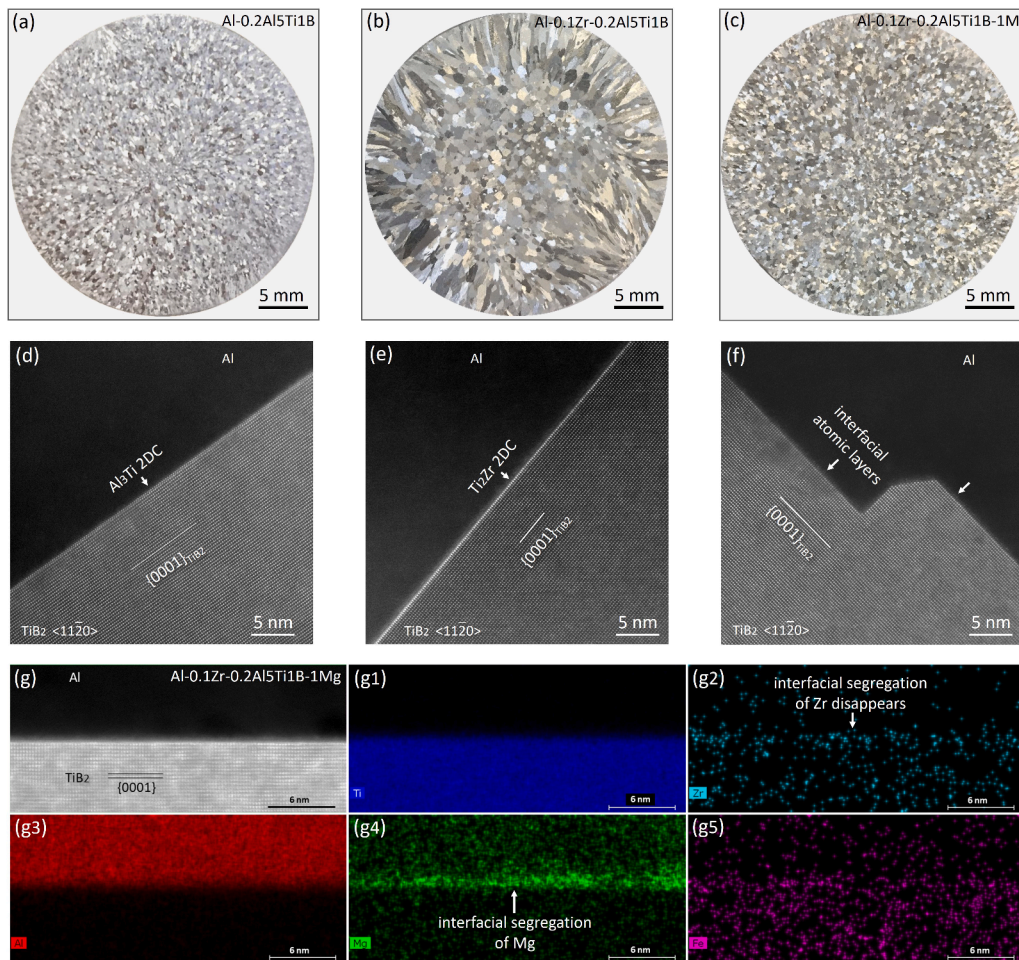

Fig. 1. Mitigation of Zr-poisoning by the interfacial segregation of Mg at the TiB$_2$/Al interface. (a-c) Optical macrographs of (a) Al-0.2Al5Ti1B; (b) Al-0.1Zr-0.2Al5Ti1B; and (c) Al-0.1Zr-0.2Al5Ti1B-1Mg. (d-f) HAADF STEM images showing the interfacial segregation layer(s) at the TiB$_2$/Al interfaces in the corresponding samples of (a-c), as viewed along the $< 11\bar{2}0 >_{TiB_2}$ zone axis. (g) Segregation of Mg illustrated by STEM-EDS elemental maps of Ti (g1), Zr (g2), Al (g3), Mg (g4), and Fe (g5) across the TiB$_2$/Al interface in sample Al-0.1Zr-0.2Al5Ti1B-1Mg.

do not affect the shape and size of TiB$_2$ particles. Moreover, the previous work [19] showed that, once TiB$_2$ becomes impotent due to the Zr-poisoning, increasing the growth restriction can not refine the solidified grains. By excluding these factors, we posit that the atomic-scale modification at the TiB$_2$/Al interface accounts for the grain-refining behaviour depicted in Fig. 1.

Fig. 2(a-c) readily shows striking microstructural differences in the atomic-resolution HAADF STEM images across TiB$_2$/Al interfaces among the three samples: the control Al-0.2Al5Ti1B, the poisoned Al-0.1Zr-0.2Al5Ti1B, and the rejuvenated Al-0.1Zr-0.2Al5Ti1B-1Mg.

In Al-0.2Al5Ti1B, a monolayer of Al$_3$Ti 2DC is seen at the TiB$_2$/Al interface (Fig. 2(a)), exhibiting a slightly lower brightness than the Ti columns in the TiB$_2$ matrix. Above this, another two less-intense atomic layers (labelled #12–13, the second being more diffuse) are observed. They are assumed to be mainly comprised of Al, which would be inherited from liquid layering during prenucleation [18,35,36]. Similar atomic layering features can be recognised in the results from prior reports, albeit not identified nor explicitly commented on [17,21,22]. Furthermore, in another system, a similar structure of Al-transition layers was reported at the TiC$_x$/Al interface [37]. Unlike the Ti atomic layers in TiB$_2$, which stack coincidently along the [0001]$_{TiB2}$ axis, the Al$_3$Ti 2DC monolayer shifts to a different lattice site. From this Ti-rich layer upward, the atomic layers (#11–13) stack in a manner following the face-centered-cubic (FCC) type. The interplanar spacing (*d*-spacing) was measured for each labelled layer as the distance to the layer

beneath. As shown in Fig. 2(a1), the *d*-spacings are 0.208 ± 0.011 nm and 0.214 ± 0.021 nm for layer #12 and #13, respectively. As suggested by the larger error bars, they have a lower degree of in-plane order than that of the TiB$_2$ matrix.

In the poisoned Al-0.1Zr-0.2Al5Ti1B, however, the Al$_3$Ti 2DC disappears and the Ti$_2$Zr 2DC forms instead as the result of Zr interfacial segregation (Fig. 2(b)). In the Ti$_2$Zr 2DC monolayer (#10), Zr atoms occupy the Ti sites of TiB$_2$ with positional deviation, appearing as elliptical columns of higher brightness than the pure Ti columns. Here, a dull atomic layer #11 not obeying the FCC stacking sequence appears 0.184 ± 0.007 nm above the Zr-rich layer (Fig. 2(b1)), which could be an Al-based atomic layer indicated by the image contrast. Further into the Al matrix, the contrast becomes too diffuse to be recognized as ordered atomic layers.

These results confirm once more that by tuning nucleation potency, the formation of Al$_3$Ti 2DC accounts for the grain refinement (Fig. 1(a)), while Ti$_2$Zr 2DC causes the poisoning effect (Fig. 1(b)). These findings are consistent with previous studies on this system [14,17,19].

After further adding 1 % Mg (*i.e.,* Al-0.1Zr-0.2Al5Ti1B-1Mg, Fig. 2 (c)), the Ti$_2$Zr 2DC disappears but the Al$_3$Ti 2DC is not regained at the TiB$_2$/Al interface. Instead, two clearly visible atomic layers (labelled #11–12) and another layer of faint contrast (#13) appear. Similar to the atomic layers beyond Al$_3$Ti 2DC described above, their stacking pattern changes into an FCC-type sequence. As shown in Fig. 2(c1), the measured *d*-spacings are 0.205 ± 0.008 nm for layer #11 and 0.203 ±
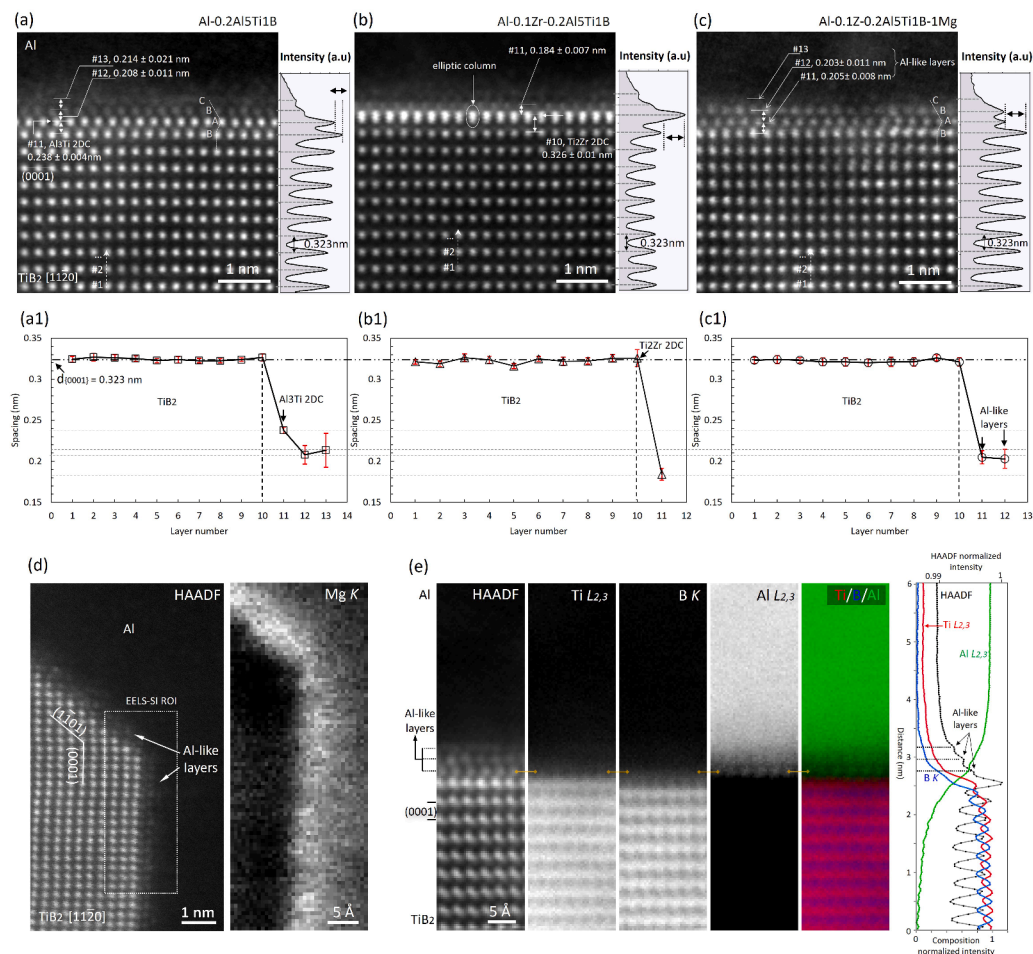

Fig. 2. (a-c) Atomic-resolution HAADF STEM images showing the atomic structure across the TiB$_2$/Al interface in samples (a) Al-0.2Al5Ti1B; (b) Al-0.1Zr-0.2Al5Ti1B; and (c) Al-0.1Zr-0.2Al5Ti1B-1Mg. (a1-c1) The corresponding interplanar spacings across the interface are statistically measured by Atomap [38]. In an interested atomic layer the spacing between every atomic column to the layer underneath is measured to gain average values and statistical errors for the interplanar spacing. (d-e) HAADF STEM images and EELS elemental maps showing the distribution of (d) Mg, (e) Ti, B, Al across the TiB$_2$/Al interface in sample Al-0.1Zr-0.2Al5Ti1B-1Mg. The incident beam is parallel to the [11$\bar{2}$0]$_{TiB_2}$ zone axis.

0.011 nm for layer #12. The EELS elemental maps in Fig. 2(d-e) offer convincing evidence that these atomic layers are an Al(Mg) solid solution as they are mainly composed of Al, in conjunction with some segregation of Mg. In Fig. 2(e), atomic columns are clearly resolved in the Al $L_{2,3}$ map, in direct spatial correlation to the corresponding depleted columns observed in either the core-loss Ti $L_{2,3}$ or B K maps. The corresponding HAADF and compositional profiles averaged across the width of the interface further demonstrate this chemical assignment. Given the observed stacking type, d-spacings, and compositions, we propose to name such an interfacial complexion (#11–13) as Al-like layers, which also show structural and compositional similarities to the layers (#12–13) observed above Al_3Ti 2DC (Fig. 2(a1)) in the Al-0.2Al5Ti1B sample.

Reproducible orientation relationships (ORs) are readily found between TiB_2 and α-Al leading to the formation of low-energy interfacial configuration when TiB_2 are potent substrates for the nucleation of α-Al [13,14,17,40]. In contrast, such ORs are not observed when TiB_2 gets poisoned by either the segregation of Zr or Si [19–21]. In conjunction with the rejuvenated grain refinement, well-defined ORs have been repeatedly found between TiB_2 and α-Al in Al-0.1Zr-0.2Al5Ti1B-1Mg, with typical examples demonstrated in Fig. 3. By indexing the selected area electron diffraction (SAED) patterns and HRTEM lattice images, the OR1 is identified as: $(0001)_{TiB2}$ // $(\overline{1}1\overline{1})_{Al}$, $[11\overline{2}0]_{TiB_2}$ // $[011]_{Al}$, while OR2 is: $(0001)_{TiB2}$ ~2° from $(200)_{Al}$, $[11\overline{2}0]_{TiB_2}$ // $[011]_{Al}$. Within experimental errors, they are consistent with previously reported ORs [13,14,17,40,41]. The application of Zhang's $\Delta \vec{g}$ theory [39] to the SAED patterns suggests that both TiB_2/Al interfaces achieve interfacial energy minima under the two ORs from a crystallographic point of view. Specifically, OR1 satisfies the **Rule I** in Ref. [39] that $\Delta \vec{g}$ is parallel to a rational $\vec{g}$ (Fig. 3(a1)): $\Delta \vec{g}_1 = \vec{g}_{(\overline{1}1\overline{1})Al} - \vec{g}_{(0001)TiB2}$ is parallel to $\vec{g}_{(0001)TiB2}$ and also to $\vec{g}_{(\overline{1}1\overline{1})Al}$. For OR2, there exist three $\Delta \vec{g}s$ parallel to each other (Fig. 3(b1)), which meets the parallelism criterion **Rule II** in Ref. [39]. The reappearing ORs satisfying the $\Delta \vec{g}$ criteria strongly suggest that TiB_2 in Al-0.1Zr-0.2Al5Ti1B-1Mg has been reactivated again as nucleation sites .

The atomic-resolution HAADF STEM images in Fig. 4(a-b) compare the TiB_2/Al_3Ti-2DC/Al and TiB_2/Al-like layers/Al interfaces that obey the OR1 after nucleation and solidification. In both cases, an edge-type misfit dislocation occurs on the Al side to compensate for the lattice mismatch. Structural relaxation appears beneath the dislocation core, specifically at the first Al-rich layer (labelled "layer 1") of less-defined, or "fuzzy" contrast illustrated in Fig. 4(c, d). The d-spacing of "layer 1" remains smaller than $d_{\{111\}Al}$, but becomes identical to $d_{\{111\}Al}$ for all atomic layers upwards. In interfacial regions away from the dislocation (Fig. 4(e, f)), the FCC-type stacking sequence continues towards the Al matrix. Comparing the interfacial structures to the ones in Fig. 2(a, c), we can attribute the lattice-misfit accommodation during α-Al nucleation to the structural relaxation of the extra layers above Al_3Ti 2DC or of the Al-like layers. On the contrary, the Al_3Ti 2DC does not directly accommodate the lattice misfit as it remains coherent with TiB_2 after nucleation (Fig. 4a), in identical fashion to the Al_3Ti 2DC in Fig. 2(a) without triggering heterogeneous nucleation. This is different from previous reports where the monolayer Al_3Ti 2DC was suggested to initiate dislocation for strain relaxation [16,18].

The best possible nucleant for α-Al nucleation would be the solid Al itself [42]. Moreover, as indicated by the close characteristics of the Al-like layers to the extra Al-rich layers above the well-known potent Al_3Ti 2DC, here we propose that they catalyse the nucleation process by providing a template of a close nature to the Al solid. This mechanism suggests that the Ti_2Zr 2DC, although coherent with TiB_2 as the other 2DCs (Fig. S5), is not potent at all since the ordered layer above does not obey the FCC-stacking pattern. It is important to note that this proposed mechanism assumes that the crystalline adsorbates appear in the melts and are preserved after solidification. This follows the suggestion of Jones's hypernucleation theory [8]. Some evidence from the literature supports this assumption. Firstly, Al_3Ti 2DC and the adsorbates above are structurally comparable to the structures found above the TiB_2 embedded in an Al-based glassy matrix after rapid solidification [14], in which the early-stage nucleation is preserved for observation. If they had developed during cooling in the solid state, we would expect structural differences because of the vastly different dynamics at different cooling rates. Secondly, the adsorbates' ordering degree decays
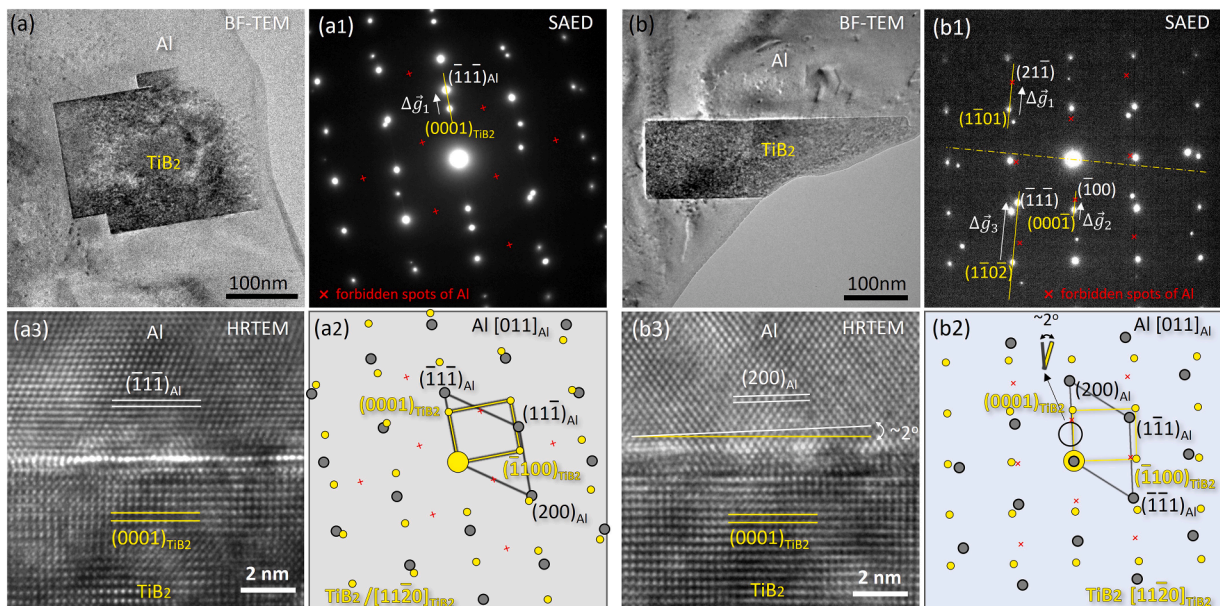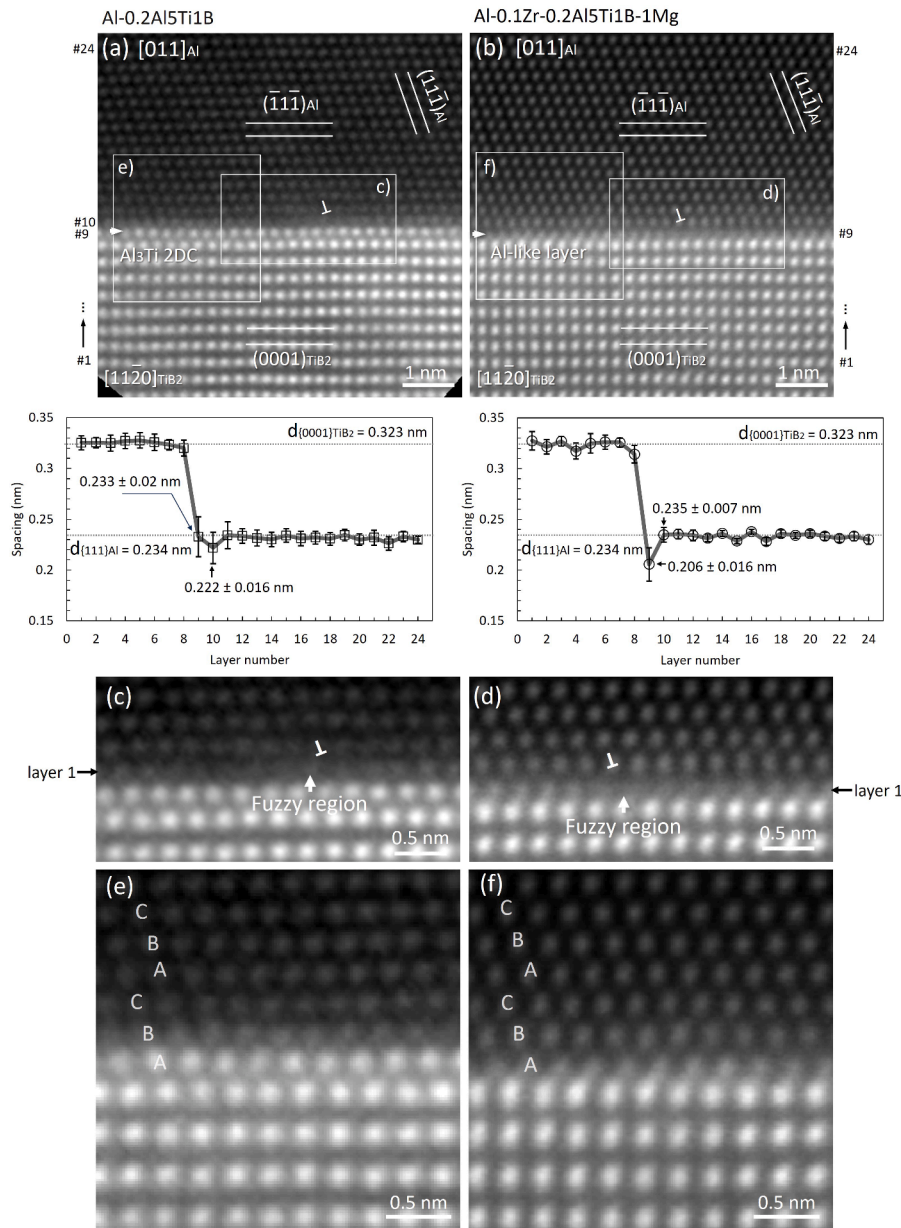

Fig. 3. Electron microscopy characterisation of BF-TEM, selected area electron diffraction (SAED), and HRTEM showing two well-defined orientation relationships (ORs) between TiB_2 and Al in the sample of Al-0.1Zr-0.2Al5Ti1B-1Mg, with the incident beam parallel to the $[11\overline{2}0]_{TiB_2}$ zone axis. (a) OR1: $(0001)[11\overline{2}0]_{TiB_2}$ // $((\overline{1}1\overline{1})_{Al})[011]_{Al}$; and (b) OR2: (0001) $[11\overline{2}0]_{TiB_2}$ // $(200)[011]_{Al}$. The two ORs satisfying either Δ**g**s parallelism criterion [39] (a) I or (b) II suggest that the poisoned TiB_2 particles by Zr segregation have been reactivated for heterogeneous nucleation after the addition of 1 % Mg. Alternatively, OR2 can be treated as the refinement of OR1 by rotating the Al pattern by ~52° to meet Δ**g**s parallelism criterion.

Fig. 4. Atomic-resolution HAADF STEM images and the measured interplanar spacings across the TiB$_2$/Al interfaces possessing OR1. (a, c, e) TiB$_2$/Al$_3$Ti-2DC/Al interface in Al-0.2Al5Ti1B; and (b, d, f) TiB$_2$/Al-like layers/Al interface in Al-0.1Zr-0.2Al5Ti1B-1Mg. (c, d) Enlarged areas containing a misfit dislocation. (e, f) Enlarged areas free of misfit dislocation on the Al side, with marks of "ABCA…" showing the FCC-type stacking pattern. Note that the incident beam is parallel to $[11\bar{2}0]_{TiB_2}$. After the nucleation of Al solid, the Al$_3$Ti 2DC monolayer (#9 in (a)) remains coherent with the TiB$_2$. At the interfaces, local structural relaxation occurs primarily (c) in the first layer (#10 in (a)) above Al$_3$Ti 2DC or (d) in the first Al-like layer (#9 in (b)), both of which are labelled "layer 1" in (c) and (d).

with distance from the interface, which is a feature typical of liquid ordering [36,43]. Lastly, the Al-like layers offer a remarkable similarity to the ordered structure at a TiB$_2$/Al-liquid interface simulated by *ab initio* molecular dynamics above the melting point [18,35]; the ordering process may cease and remain even if eventually nucleation is not triggered on this substrate. Nevertheless, and despite the similarities and correlations highlighted here, we should bear in mind that any structure observed postmortem is by definition not the same as that present in the liquid due to temperature differences, and these results should thus be seen as insights into the solidification process.

Dissolution of Mg in Al causes lattice expansion [44]. With the interfacial segregation of Mg, the lattice of the Al(Mg) solution expands to reduce the lattice misfit with TiB$_2$, which could also facilitate the formation of Al-like layers and the subsequent nucleation of α-Al. The structural compatibility is further improved when considering thermal

expansion at the nucleation temperature. As demonstrated in Fig. S6, the lattice misfit decreases as the Mg concentration and temperature increase. Therefore, adding Mg into a Al melt with TiB$_2$ inoculation will be beneficial for grain refinement because of both the improved potency (if segregation occurs) and growth restriction effect, a conclusion consistent with the fact that no poisoning by Mg has ever been observed [45].

In summary, we have demonstrated through casting experiments that adding Mg can revive grain refinement from the Zr-poisoning effect. In the presence of Mg, the poisoned TiB$_2$ particles are re-activated for the heterogeneous nucleation of Al grains, possessing well-defined ORs with the surrounding Al. Dedicated STEM and EELS analyses provide the basis for a proposed underpinning mechanism whereby TiB$_2$ particles are modified by the interfacial segregation of Mg, which allows the dissolution of the poisoning Ti$_2$Zr 2DC and the formation of Al-like layers that act as "good" template to catalyse the nucleation of Al solid.

CRediT authorship contribution statement

Shihao Wang: Writing – original draft, Validation, Methodology, Investigation, Formal analysis, Data curation. **Yun Wang:** Writing – review & editing, Validation, Supervision, Resources, Methodology, Formal analysis, Conceptualization. **Yijie Zhang:** Writing – review & editing, Validation, Investigation, Formal analysis, Data curation. **Feng Wang:** Writing – review & editing, Validation, Methodology, Formal analysis. **Teruo Hashimoto:** Writing – review & editing, Investigation, Data curation. **Xiaorong Zhou:** Writing – review & editing, Resources. **Zhongyun Fan:** Writing – review & editing, Validation, Supervision, Resources, Funding acquisition, Conceptualization. **Quentin Ramasse:** Writing – review & editing, Validation, Supervision, Methodology, Investigation, Funding acquisition, Formal analysis, Data curation.

Declaration of competing interest

The authors declare that they have no known competing financial interests or personal relationships that could have appeared to influence the work reported in this paper.

Acknowledgements

Supplementary materials

Supplementary material associated with this article can be found, in the online version, at doi:10.1016/j.scriptamat.2024.116310.

References

[1] D.G. McCartney, Grain refining of aluminium and its alloys using inoculants, Int. Mater. Rev. 34 (1989) 247–260.
[2] B.S. Murty, S.A. Kori, M. Chakraborty, Grain refinement of aluminium and its alloys by heterogeneous nucleation and alloying, Int. Mater. Rev. 47 (2002) 3–29.
[3] D.A. Granger, J.F. Grandfield, Microstructure control in ingots of aluminum alloys with an emphasis on grain refinement, in: Essential Readings in Light Metals, 3, Springer, 2016, pp. 354–365. Cast Shop for Aluminum Production.
[4] A. Cibula, A. Clibula, The mechanism of grain refinement of sand castings in aluminium alloys, J. Inst. Met. 76 (1949) 321–360.
[5] A.L. Greer, Overview: application of heterogeneous nucleation in grain-refining of metals, J. Chem. Phys. 145 (2016) 211704.
[6] A. Cibula, The grain refinement of aluminium alloy castings by additions of titanium and boron, J. Inst. Met. 80 (1951).
[7] F.A. Crossley, L.F. Mondolfo, Mechanism of grain refinement in aluminum alloys, JOM 3 (1951) 1143–1148.
[8] G.P. Jones, Grain refinement of castings using inoculants for nucleation above liquidus, Solidif. Process. (1987) 496–499, 1987.
[9] M. Vader, J. Noordegraaf, P.C. van Wiggen, Aluminum master alloys with reduced intermetallic phase sizes open up windows for new applications, in: E.L. Rooy (Ed.), Aluminum master alloys with reduced intermetallic phase sizes open up windows for new applications, Light Met (1991) 1123–1130, 1991.
[10] L. Bäckerud, P. Gustafson, M. Johnsson, Grain refining mechanisms in aluminum as a result of additions of titanium and boron, part II, Aluminium 67 (1991) 910–915.
[11] G.K. Sigworth, Communication on mechanism of grain refinement in aluminum, Scr. Mater. 34 (1996) 919–922.
[12] P.S. Mohanty, J.E. Gruzleski, Mechanism of grain refinement in aluminium, Acta Metall. Mater. 43 (1995) 2001–2012.
[13] M. Zhang, P.M. Kelly, M.A. Easton, J.A. Taylor, Crystallographic study of grain refinement in aluminum alloys using the edge-to-edge matching model, 53 (2005) 1427–1438.
[14] P. Schumacher, A.L. Greer, J. Worth, P.V. Evans, M.A. Kearns, P. Fisher, A. H. Green, New studies of nucleation mechanisms in aluminium alloys: implications for grain refinement practice, Mater. Sci. Technol. 14 (1998) 394–404.
[15] Y. Han, Y. Dai, D. Shu, J. Wang, B. Sun, First-principles calculations on the stability of Al/TiB2 interface, Appl. Phys. Lett. 89 (2006) 144107.
[16] T. Qin, Z. Fan, Reconstruction of 2D Al3Ti on TiB2 in an aluminium melt, IOP Conf. Ser. Mater. Sci. Eng. 27 (2012) 012004.
[17] Z. Fan, Y. Wang, Y. Zhang, T. Qin, X.R. Zhou, G.E. Thompson, T. Pennycook, T. Hashimoto, Grain refining mechanism in the Al/Al-Ti-B system, Acta Mater 84 (2015) 292–304.
[18] S. Ma, N. Zong, Z. Dong, Y. Hu, T. Jing, Y. Li, R.H. Mathiesen, H. Dong, Ti-adsorption induced strain release in promoting α-Al nucleation at TiB2 - Al interfaces, Appl. Surf. Sci. 639 (2023) 158185.
[19] Y. Wang, C.M. Fang, L. Zhou, T. Hashimoto, X. Zhou, Q.M. Ramasse, Z. Fan, Mechanism for Zr poisoning of Al-Ti-B based grain refiners, Acta Mater 164 (2019) 428–439.
[20] Y. Wang, Z. Que, T. Hashimoto, X. Zhou, Z. Fan, Mechanism for Si poisoning of Al-Ti-B grain refiners in Al-Alloys, Metall. Mater. Trans. A. 51 (2020) 5743–5757.
[21] Y. Li, B. Hu, B. Liu, A. Nie, Q. Gu, J. Wang, Q. Li, Insight into Si poisoning on grain refinement of Al-Si/Al-5Ti-B system, Acta Mater 187 (2020) 51–65.
[22] D. Li, X. Yan, Y. Fan, G. Liu, J. Nie, X. Liu, S. Liu, An anti Si/Zr-poisoning strategy of Al grain refinement by the evolving effect of doped complex, Acta Mater 249 (2023) 118812.
[23] S. Wang, Y. Wang, Q.M. Ramasse, R. Schmid-Fetzer, Z. Fan, Segregation of yttrium at the Mg/MgO interface in an Mg-0.5Y alloy, Acta Mater 257 (2023) 119147.
[24] S. Wang, Characterisation of Native MgO and Its Roles in Solidification of Mg alloys, Brunel University, 2020. PhD thesis.
[25] Y. Wang, S. Wang, Z. Que, C. Fang, T. Hashimoto, X. Zhou, Q.M. Ramasse, Z. Fan, Manipulating nucleation potency of substrates by interfacial segregation: an overview, Metals (Basel) 12 (2022) 1636.
[26] C. Fang, Z. Fan, Segregation of alkaline earth atoms affects prenucleation at ʟ-Al/γ-alumina interfaces, Metals (Basel) 13 (2023) 761.
[27] L. Wang, W. Lu, Q. Hu, M. Xia, Y. Wang, J. Li, Interfacial tuning for the nucleation of liquid AlCu alloy, Acta Mater 139 (2017) 75–85.
[28] S. Ma, Z. Dong, N. Zong, T. Jing, H. Dong, Solute-adsorption enhanced heterogeneous nucleation: the effect of Cu adsorption on α-Al nucleation at the sapphire substrate, Phys. Chem. Chem. Phys. 23 (2021) 5270–5282.
[29] M.E.J. Birch, P. Fisher, Grain refining of commercial aluminium alloys with titanium boron aluminium, Alum. Technol. 86 (1986) 117–124.
[30] G.P. Jones, J. Pearson, Factors affecting the grain-refinement of aluminum using titanium and boron additives, Metall. Trans. B. 7 (1976) 223–234.
[31] H. Yang, Z. Qian, G. Zhang, J. Nie, X. Liu, The grain refinement performance of B-doped TiC on Zr-containing Al alloys, J. Alloys Compd. 731 (2018) 774–783.
[32] M.A. Kearns, P.S. Cooper, Effects of solutes on grain refinement of selected wrought aluminium alloys, Mater. Sci. Technol. 13 (1997) 650–654.
[33] T.E. Quested, A.L. Greer, The effect of the size distribution of inoculant particles on as-cast grain size in aluminium alloys, Acta Mater 52 (2004) 3859–3868.
[34] Y. Xu, D. Casari, Q. Du, R.H. Mathiesen, L. Arnberg, Y. Li, Heterogeneous nucleation and grain growth of inoculated aluminium alloys: an integrated study by in-situ X-radiography and numerical modelling, Acta Mater 140 (2017) 224–239.
[35] H.L. Zhang, Y.F. Han, W. Zhou, Y.B. Dai, J. Wang, B.D. Sun, Atomic study on the ordered structure in Al melts induced by liquid/substrate interface with Ti solute, Appl. Phys. Lett. 106 (2015) 041606.
[36] H. Men, Z. Fan, Prenucleation induced by crystalline substrates, Metall. Mater. Trans. A. 49 (2018) 2766–2777.
[37] H. Yang, Z. Qian, H. Chen, X. Zhao, G. Han, W. Du, X. Nie, K. Zhao, G. Liu, Q. Sun, T. Gao, J. Zhou, J. Nie, X. Liu, A new insight into heterogeneous nucleation mechanism of Al by non-stoichiometric TiCx, Acta Mater 233 (2022) 117977.
[38] M. Nord, P.E. Vullum, I. MacLaren, T. Tybell, R. Holmestad, Atomap: a new software tool for the automated analysis of atomic resolution images using two-dimensional Gaussian fitting, Adv. Struct. Chem. Imaging. (2017) 3.
[39] W.Z. Zhang, G.C. Weatherly, On the crystallography of precipitation, Prog. Mater. Sci. 50 (2005) 181–292.
[40] J.A. Marcantonio, L.F. Mondolfo, Nucleation of aluminium by several intermetallic compounds, J Inst Met 98 (1970) 23–27.
[41] P.L. Schaffer, D.N. Miller, A.K. Dahle, Crystallography of engulfed and pushed TiB2 particles in aluminium, Scr. Mater. 57 (2007) 1129–1132.
[42] A.L. Greer, Supercool order, Nat. Mater. 5 (2006) 13–14.
[43] S.H. Oh, Y. Kauffmann, C. Scheu, W.D. Kaplan, M. Rühle, Ordered liquid aluminum at the interface with sapphire, Science 310 (2005) 661–663.
[44] W.B. Pearson, Lattice Spacings and Structures of Metals and Alloys, I II, Pergamon Press, Oxford, 1958. Vols1964, 1967.
[45] J.A. Spittle, S. Sadli, Effect of alloy variables on grain refinement of binary aluminium alloys with Al–Ti–B, Mater. Sci. Technol. 11 (1995) 533–537.